Optics Letters

In situ x-ray-induced acoustic computed tomography with a contrast agent: a proof of concept

Seongwook Choi,[1] Sinyoung Park,[1] Ayoung Pyo,[2] Dong-Yeon Kim,[3] Jung-Joon Min,[4] Changho Lee,[4,5,6] and Chulhong Kim[1,7]

[1]Department of Electrical Engineering, Convergence IT Engineering, and Mechanical Engineering, Medical Device Innovation Center, Pohang University of Science and Technology, Pohang, Republic of Korea
[2]Korea Atomic Energy Research Institute, Jeongeup, Republic of Korea
[3]College of Pharmacy and Research Institute of Pharmaceutical Science, Gyeongsang National University, Jinju, Republic of Korea
[4]Department of Nuclear Medicine, Chonnam National University Medical School & Hwasun Hospital, Hwasun, Chonnam, Republic of Korea
[5]Department of Artificial Intelligence Convergence, Chonnam National University, Gwangju, Republic of Korea
[6]e-mail: ch31037@jnu.ac.kr
[7]e-mail: chulhong@postech.edu

Received 5 November 2021; revised 24 November 2021; accepted 29 November 2021; posted 1 December 2021; published 20 December 2021

X-ray-induced acoustic computed tomography (XACT) has shown great potential as a hybrid imaging modality for real-time non-invasive x-ray dosimetry and low-dose three-dimensional (3D) imaging. While promising, one drawback of the XACT system is the underlying low signal-to-noise ratio (SNR), limiting its *in vivo* clinical use. In this Letter, we propose the first use of a conventional x-ray computed tomography contrast agent, Gastrografin, for improving the SNR of *in situ* XACT imaging. We obtained 3D volumetric XACT images of a mouse's stomach with orally injected Gastrografin establishing the proposal's feasibility. Thus, we believe, in the future, our proposed technique will allow *in vivo* imaging and expand or complement conventional x-ray modalities, such as radiotherapy and accelerators.

https://doi.org/10.1364/OL.447618

X-ray-induced acoustic computed tomography (XACT) has great potential as a novel hybrid imaging modality that combines x-ray absorption contrast with ultrasonic resolution [1–10]. The basic principle of three-dimensional (3D) XACT imaging is as follows. When an x-ray pulse illuminates a target, the target absorbs the x-ray energy. The target then goes through thermoelastic expansion resulting in acoustic emission, also called the x-ray-induced acoustic (XA) effect. The generated XA waves propagate omnidirectionally and are captured by an ultrasound (US) detector. The captured XA signals are then reconstructed to form a 3D volumetric image. The XACT system has the following unique properties. First, the strength of XA signals is directly proportional to the deposited x-ray dose. Hence, XACT is useful for monitoring dose delivery in radiation therapy and tracking the x-ray beam [5,9]. Zhang *et al*. developed dual-modality XA and US imaging for real-time monitoring of radiotherapy in biological samples [11]. Second, the strength of generated XA signals is proportional to the x-ray absorption density of the target. Thus, XACT can be used for measuring material densities. Li *et al*. and Robertson *et al*. implemented and simulated XACT bone imaging to evaluate potential bone diseases [12,13]. Third, XACT provides 3D information using only a single x-ray pulse. Thus, XACT requires a lower radiation dose than conventional x-ray computed tomography (CT) [14,15], potentially benefiting patient care.

In our previous work, we presented a 3D volumetric XACT system for the first time [16,17]. The study established the feasibility of 3D volumetric XACT using lead targets but did not verify *in vivo* or *in situ* conditions. In this study, we demonstrate *in situ* 3D volumetric XACT of small animals using the contrast agent Gastrografin, a conventional x-ray CT contrast agent made for gastrointestinal (GI) tract monitoring. We used a contrast agent to improve the signal-to-noise (SNR) of the XACT system. We first acquired the 3D XACT images of Gastrografin with 1.5 ml e-tubes. Then the contrast agent was injected orally to visualize the mouse's GI tract. We could successfully obtain the *in situ* mouse XACT image and compare it against an x-ray CT image. The comparison results confirm that 3D XACT can be expanded to the biomedical imaging field. In the next few paragraphs, we describe the system and the experimental setup.

The experimental schematic of the system is shown in Fig. 1. The control room was separated from the experimental room by using lead x-ray shielding walls to protect from radiation exposure. The personal computer (PC), which controlled the motor and all other experimental setups, and the x-ray switch were in the control room. The rest of the equipment, including the x-ray source, imaging target, and array transducer, were in the x-ray shielding room. The portable x-ray source (XR200, Golden Engineering, USA) provided the pulsed x-ray beam with a pulse width of 50 ns, a repetition frequency of 10 Hz, a tube potential of 150 kVp, and a beam angle of 40°. When the pulsed x-ray beam illuminated the imaging target, the target started generating XA signals, which were acquired by an arc-shaped US transducer (12645–1001, Imasonics SAS, France) with a radius curvature of 65 mm, 96 elements, central frequency of

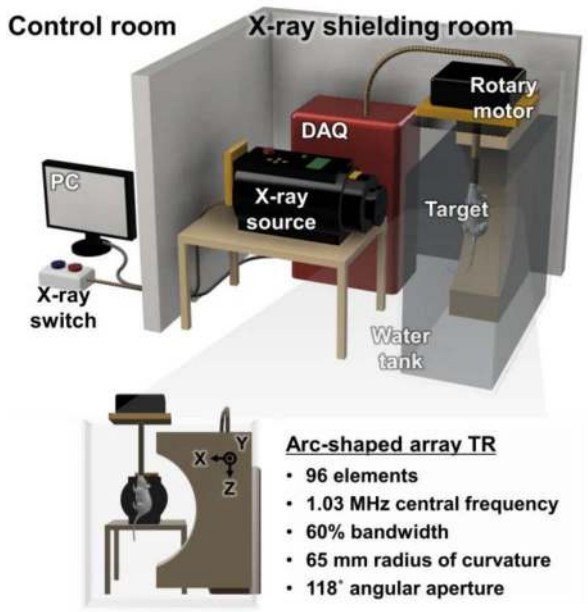

Fig. 1. Schematic of XACT system: TR, transducer; DAQ, data acquisition board.

1.03 MHz, –6 dB bandwidth of 60%, and an active angular aperture of 118°. Each element of the transducer had an active area of 1.3 mm × 1.3 mm, a pitch size of 1.4 mm, and a spacing of 0.1 mm. The portable x-ray source could shoot up to 200 pulses in 4 min. The data acquisition board (DAQ; Photosound Inc., USA) had 96 parallel analog-to-digital converter channels with 12-bit resolution and was integrated with a rotary piezo motor and control software for scanning the imaging target. The DAQ was synchronized using the external trigger from a photodiode and scintillator (PDA36A-EC, Thorlabs, USA). The scintillator changed the x-ray beam to visible light, then the photodiode could make the trigger by detecting this visible light. The imaging target was hung on the rotary motor, and the rotary motor waited for the average number of pre-set shots to be collected before rotating by a specified angle. The DAQ acquired 3072 A-line samples of the XA signal at a sampling frequency of 31.25 MHz for each transducer element.

At first, we determined the relationship between the SNRs of the XA signals and various conditions of the contrast agent Gastrografin (Bayer, Germany). To prepare the concentrated contrast agent, the original Gastrografin (oG, 100 ml) was transferred to a single neck round bottom flask and evaporated under reduced pressure to remove the solvent. Then, hot water (50 ml) was added to the dried Gastrografin and stirred for 20 min. Finally, twice concentrated Gastrografin (cG) was passed through a membrane filter into a 1.5 ml e-tube for further evaluation [Fig. 2(b)]. In addition, we also evaluated the e-tube embedded in chicken tissue (a cuboid of 28 mm × 28 mm × 40 mm) to verify the feasibility of *in vivo* or *in situ* conditions in chicken tissue. For each of the four cases (i.e., water, oG, cG, cG in chicken tissue), we obtained 200 data points from one angle without scanning and averaged them. For comparison, SNRs were calculated by dividing the highest XA signal by the root-mean-square of noise in the A-line data of one element channel. The calculated mean SNRs of the array transducer are shown in Fig. 2(a). The results show that the cG's SNR (21.36 dB) was higher than the oG's

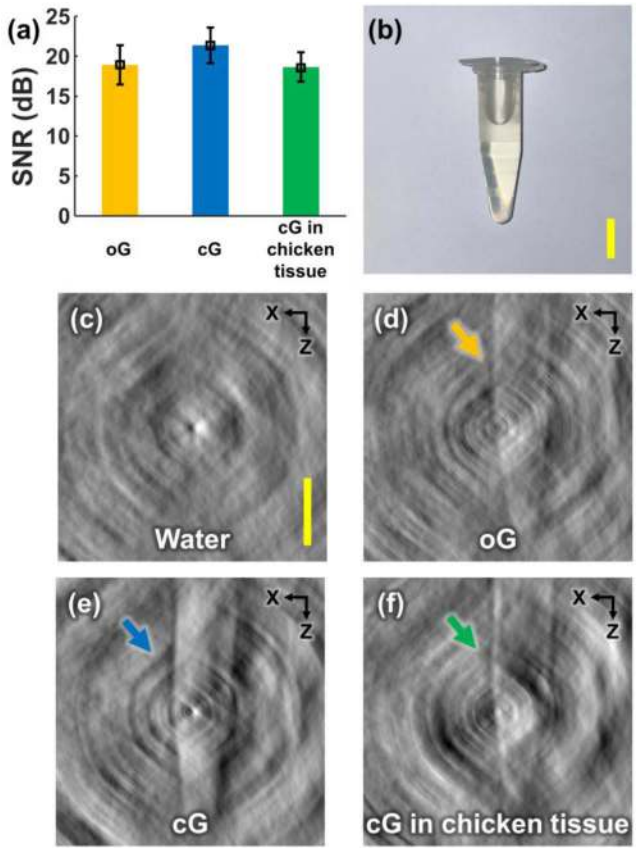

Fig. 2. (a) SNRs versus various Gastrografin conditions. (b) Photograph of material in the e-tube. Cross-section XACT images of (c) water, (d) oG, (e) cG, and (f) cG in chicken tissue. The yellow scale bar is 10 mm. Chicken tissue size is 28 mm × 28 mm × 40 mm [width (X) × length (Y in Fig. 1) × height (Z)].

SNR (18.91 dB) and the cG's SNR in chicken tissue (18.65 dB). For the Gastrografin targets, we could see the boundaries of the e-tubes, while no boundary was visible in the water-filled tube [Figs. 2(c)–2(f)].

For 3D phantom XACT imaging, we rotated the imaging target (i.e., the 1.5 ml e-tube), using the rotary motor at an angle interval of 8°. The average number of images acquired was approximately 200; this figure was not exact due to the x-ray source's inherent instability. The acquired raw data were interpolated eight times around the rotation axis to obtain data at every degree of rotation angle. These post-processed data were reconstructed to form a 3D volumetric XACT image using the GPU-accelerated back-projection algorithm discussed in the previous study [16]. Briefly, the CPU (i7-4790, Intel, USA) calculates the reconstructed volume coordinates and the transducer's position and preprocesses the raw data. For all 3D XACT imaging, the reconstructed volume was 40 mm × 40 mm × 40 mm with a voxel size of 0.1 mm. The GPU (GTX-960, NVIDIA, USA) software has three kernels to process: 3D sample map, data projection/summation, and reconstruction of 3D volume data. Using this software, we successfully obtained the XACT images of all four cases: e-tubes filled with oG, oG in chicken tissue, cG, and cG in chicken tissue (Fig. 3). The chicken tissue size was 28 mm × 28 mm × 40 mm [width (X) × length (Y) × height (Z)]. The reconstructed 3D XACT images were rendered using the 3D PHOVIS software

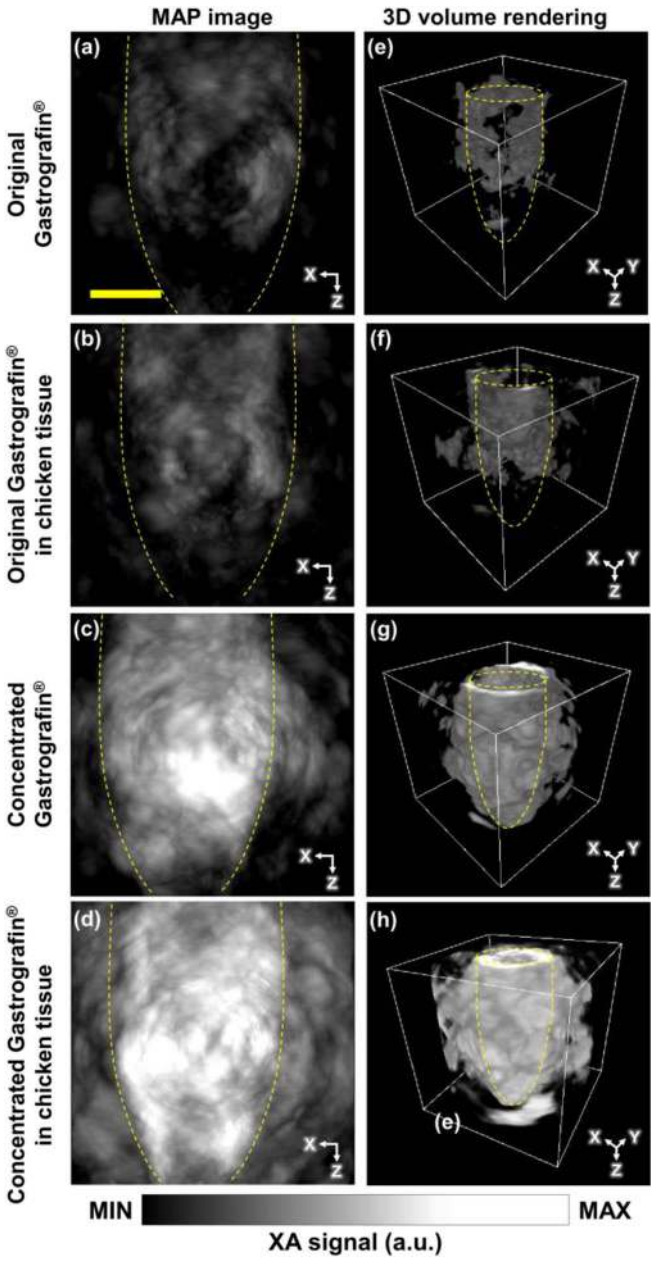

Fig. 3. (a)–(d) Two-dimensional MAP XACT images and (e)–(h) 3D volumetric rendering of various phantoms. The yellow scale bar is 10 mm. Chicken tissue size is 28 mm × 28 mm × 40 mm (width × length × height).

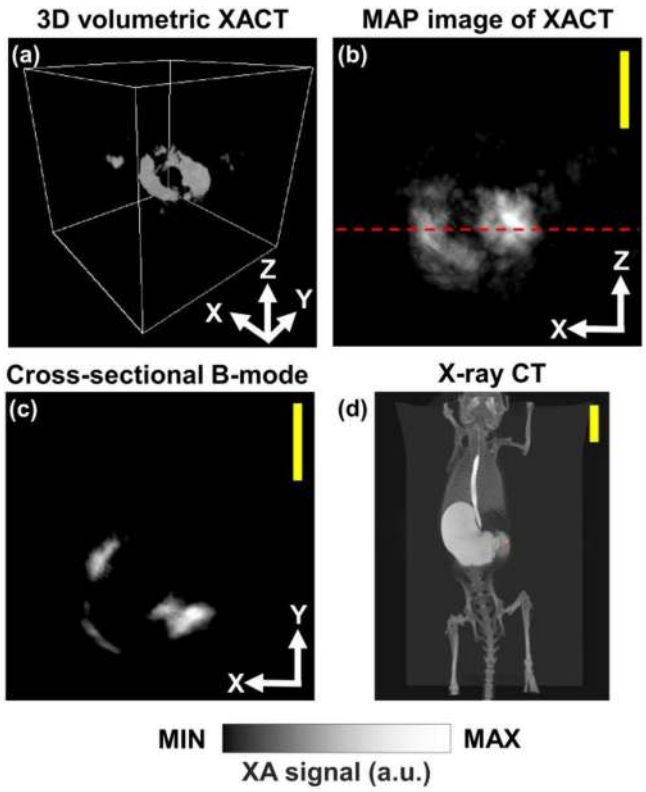

Fig. 4. (a) 3D rendered XACT image and (b) MAP image of a mouse with an oral injection of cG *in situ*. (c) Cross-sectional B-mode image of the horizontal red dashed line in (b). (d) X-ray CT of the operated-on mouse. The yellow scale bar is 10 mm.

system for visualization [18]. We set the same color bar and saturation criterion to each XACT image for a fair comparison. We could easily detect XA signals from the e-tube in the center part of each XACT volumetric image, and we could distinguish the 3D shape of the e-tubes in cG and cG in chicken tissue. However, it was difficult to determine the boundaries of the e-tubes in oG and oG in chicken tissue owing to the low SNRs. Furthermore, 3D image reconstruction could induce image artifacts because the e-tubes could not be accurately aligned with the rotation axis.

Animal care, animal experiments, and euthanasia were performed in accordance with the protocols approved by the Chonnam National University Animal Research Committee and the Guide for the Care and Use of Laboratory Animals. For *in situ* mouse imaging, we surgically tied the intestine to keep the contrast agent in the mouse's stomach. We injected the contrast agent orally into the stomach using a nasogastric tube (KN-349, Nastume, Japan). We confirmed that the contrast agent stayed in the stomach by visually observing the swollen abdomen. We then euthanized the mouse with an overdose of isoflurane before performing the XACT imaging experiments. We set the average number of image acquisition to 200 and the step interval angle to 4°. The XACT imaging took 6 h with this setup owing to the specification of the x-ray source, which could shoot up to 200 pulses in 4 min in a stable manner. The raw data were quadrupled in the rotation direction. Figures 4(a)–4(c) show the 3D XACT images of the mouse injected with the contrast agent *in situ*. To validate XACT imaging results, we also performed conventional x-ray CT (SuperArgus PET/CT, Sedecal, Spain) on the same mouse after the XACT imaging experiments. The CT images confirmed that the mouse's stomach was filled with the contrast agent [Fig. 4(d)]. Note that in the XACT images, the stomach was not entirely filled with the cG, whereas the CT image showed a completely filled stomach. This minor discrepancy could be due to air cavities present in the stomach, which would prevent the propagation of acoustic waves to the US detector.

This study explored the feasibility of 3D XACT in small animals *in situ* with the conventional x-ray CT contrast agent, Gastrografin. Our study is the first time a contrast agent has been employed with the 3D XACT to study animals *in situ*.

We compared the XA signals generated between water, oG, and cG. The SNR of the cG was about 13% higher than that of the oG. We also performed *in situ* XACT imaging experiments on small animals with orally injected Gastrografin. We validated XACT imaging results by comparing them against the findings of x-ray CT on the same animal. Although we demonstrated the proof of concept of 3D XACT mouse imaging using contrast agents, some limitations remain. XACT can theoretically acquire 3D x-ray absorption information from one single x-ray shot whereas x-ray CT cannot; however, the current XACT system still needs a large number of averages owing to the low SNR. The SNR can be further enhanced by using a hemispherical array transducer with a wider numerical aperture, which could also make real-time XACT imaging possible. In addition, because Gastrografin based on iodine is highly absorptive at the lower x-ray voltage range (tens of kiloelectron volts), an x-ray source with low energy (currently, 150 kVp) could improve the SNR and image quality. Hence, we will be able to implement *in vivo* XACT imaging using the original contrast agent with the optimal x-ray source. Another limitation is that we did not correct the inhomogeneous dose distribution induced by the x-ray beam divergence. Although we aligned the center of the x-ray tube window and the animal, the x-ray dose distribution would have been irregular because the animal was 30 cm away from the x-ray tube. If we detect or calculate the dose distribution then compensate the XA signals, XACT imaging will be more accurate.

In the future, we expect that our proposed technique will allow *in vivo* imaging and expand or complement conventional x-ray modalities, such as radiotherapy and accelerators.

Funding. Ministry of Education (2019H1A2A1076500, 2020R1A6A1A03047902); Ministry of Science and ICT, South Korea (NRF-2015M3C1A3056407, NRF-2017M3C1A3037762, NRF-2019R1A2C2006269).

Acknowledgment. We thank Su-Woong Yoo MD, Ph.D. for supporting animal surgery.

Disclosures. C. Kim has financial interests in OPTICHO, which, however, did not support this work.

Data availability. Data underlying the results presented in this paper are not publicly available at this time but may be obtained from the authors upon reasonable request.

REFERENCES

1. L. Xiang, B. Han, C. Carpenter, G. Pratx, Y. Kuang, and L. Xing, Med. Phys. **40**, 010701 (2012).
2. S. Hickling, M. Hobson, and I. El Naqa, Int. J. Radiat. Oncol., Biol., Phys. **90**, S843 (2014).
3. S. Hickling, P. Léger, and I. El Naqa, IEEE Trans. Ultrason., Ferroelect., Freq. Contr. **63**, 683 (2016).
4. L. Xiang, S. Tang, M. Ahmad, and L. Xing, Sci. Rep. **6**, 26118 (2016).
5. J. Kim, E.-Y. Park, Y. Jung, B. C. Kim, J. H. Kim, C.-Y. Yi, I. J. Kim, and C. Kim, IEEE Trans. Radiat. Plasma Med. Sci. **1**, 534 (2017).
6. S. Tang, D. Nguyen, A. Zarafshani, C. Ramseyer, B. Zheng, H. Liu, and L. Xiang, Appl. Phys. Lett. **110**, 103504 (2017).
7. S. Tang, C. Ramseyer, P. Samant, and L. Xiang, Appl. Phys. Lett. **112**, 063504 (2018).
8. S. Tang, K. Yang, Y. Chen, and L. Xiang, Med. Phys. **45**, 1662 (2018).
9. H. Lei, W. Zhang, I. Oraiqat, Z. Liu, J. Ni, X. Wang, and I. El Naqa, Med. Phys. **45**, 4191 (2018).
10. F. Forghani, A. Mahl, T. J. Patton, B. L. Jones, M. A. Borden, D. C. Westerly, C. Altunbas, M. Miften, and D. H. Thomas, Med. Phys. **47**, 1280 (2020).
11. W. Zhang, I. Oraiqat, H. Lei, P. L. Carson, I. El Naqa, and X. Wang, BME Frontiers **2020**, 9853609 (2020).
12. Y. Li, P. Samant, S. Wang, A. Behrooz, D. Li, and L. Xiang, IEEE Trans. Ultrason., Ferroelect., Freq. Contr. **67**, 1613 (2020).
13. E. Robertson, P. Samant, S. Wang, T. Tran, X. Ji, and L. Xiang, IEEE Trans. Ultrason., Ferroelect., Freq. Contr. **68**, 1073 (2021).
14. P. Samant, L. Trevisi, X. Ji, and L. Xiang, J. Photoacoust. **19**, 100177 (2020).
15. S. Choi, E.-Y. Park, S. Park, J. H. Kim, and C. Kim, Sci. Rep. **11**, 1 (2021).
16. D. Lee, E.-Y. Park, S. Choi, H. Kim, J.-j. Min, C. Lee, and C. Kim, Biomed. Opt. Express **11**, 752 (2020).
17. S. Choi, D. Lee, E.-Y. Park, J.-J. Min, C. Lee, and C. Kim, in *Photons Plus Ultrasound: Imaging and Sensing 2020*, (International Society for Optics and Photonics, 2020), 112404R.
18. S. Cho, J. Baik, R. Managuli, and C. Kim, J. Photoacoust. **18**, 100168 (2020).